



# Improvement of CO<sub>2</sub> capture processes by tailoring the reaction enthalpy of Aprotic N-Heterocyclic anion-based ionic liquids

D. Hospital-Benito, J. Lemus, C. Moya, R. Santiago, J. Palomar<sup>\*</sup>

Chemical Engineering Department, Universidad Autónoma de Madrid, 28049 Madrid, Spain

## ARTICLE INFO

### Keywords:

CO<sub>2</sub> capture  
Ionic liquids  
Cost estimation  
Process simulation  
COSMO-based/Aspen

## ABSTRACT

A wide variety of Aprotic N-Heterocyclic Anion-based Ionic Liquids (AHA-ILs) were designed using DFT/COSMO-RS quantum chemical calculations to optimize their performance as chemical absorbents on industrial-scale CO<sub>2</sub> capture processes by tailoring the enthalpy of reaction. Five different substituents located at multiple positions on eight different heterocyclic rings were considered to cover a wide range of CO<sub>2</sub>-IL reaction enthalpies. Twelve representative AHA-ILs based on [P<sub>66614</sub>] cation with an enthalpy of reaction from -30 to -64 kJ/mol were evaluated on post-combustion, biogas and pre-combustion CO<sub>2</sub> chemical capture processes through Aspen Plus Rate-based simulations. AHA-ILs presenting a CO<sub>2</sub> reaction enthalpy between -43 and -54 kJ/mol were found to minimize both solvent and energy consumptions and thus equipment and operating costs in all studied CO<sub>2</sub> capture systems, since cyclic capacity is successfully optimized by a correct selection of the reaction enthalpy. Some non-synthesized AHA-ILs, as [P<sub>66614</sub>][4-BrPyra] (-49.3 kJ/mol), are proposed as promising CO<sub>2</sub> chemical absorbents based on their enhanced performance in post-combustion, biogas and pre-combustion capture processes from current techno-economic analysis.

## 1. Introduction

Nowadays, the development of more efficient CO<sub>2</sub> capture technologies is regaining importance due to the growing biogas and H<sub>2</sub> production markets [1, 2], together with the long-contemplated Carbon Capture and Storage (CCS) or Utilization (CCU) strategies to reduce global warming [3–5].

Attention is paid in several gas separation techniques, highlighting absorption, adsorption, and membrane separation because their industrial relevance [3, 6]. Research efforts are focused on both developing new advanced materials with enhanced CO<sub>2</sub> capture performance and investigating more efficient processes with optimized flow-schemes and operating conditions, to minimize chemicals and energy consumption, process cost and environmental impact [6–12].

In this sense, ionic liquids (ILs) are promising candidates for CO<sub>2</sub> capture due to their favorable properties like good CO<sub>2</sub> solubility, low volatility and high thermal stability. ILs physically absorbing CO<sub>2</sub> were firstly proposed, but drawbacks like high molecular weight and viscosity hinder their industrial implementation. To address these problems, ILs were functionalized to upgrade the CO<sub>2</sub> absorption performance by introducing reactive functional groups [3, 4]. Chemically absorbing CO<sub>2</sub>

using ionic liquids (ILs) is being investigated as alternative to current technology based on an aqueous amine solution, since they avoid solvent losses and reduce energy duty and operating and investment costs in post-combustion, biogas and pre-combustion processes [4, 8, 10, 13–15]. Aprotic N-Heterocyclic Anion-based ionic liquids (AHA-ILs) are reported as promising CO<sub>2</sub> chemical absorbents, due to their negligible volatility, favorable IL-CO<sub>2</sub> reaction stoichiometry, high CO<sub>2</sub> uptake capacity, relatively low heat of reaction, high chemical and thermal stability and relatively low viscosity (which does not increase by reaction with CO<sub>2</sub>) [16–18]. A main advantage of AHA-ILs is their tunable molecular structure, which can be conveniently modified to improve the solvent properties on CO<sub>2</sub> capture [18–20]. Indeed, some AHA-ILs based on imide anions were recently found to even reach superior 2:1 absorption capacity by the adequate combination of chemical and physical absorption [21]. Thus, the enthalpy of CO<sub>2</sub>+AHA-IL reaction plays a main role in process performance, being demonstrated that increasing the reaction exothermicity can enhance solvent and energy requirements, consequently reducing overall process costs [13, 22–24].

In this work, a multiscale computational approach was applied to design new AHA-ILs with enhanced process performance as CO<sub>2</sub> chemical absorbents in post-combustion, biogas and pre-combustion

<sup>\*</sup> Corresponding author.

E-mail address: [pepe.palomar@uam.es](mailto:pepe.palomar@uam.es) (J. Palomar).

<https://doi.org/10.1016/j.cej.2022.100291>

Received 21 January 2022; Received in revised form 24 February 2022; Accepted 16 March 2022

Available online 21 March 2022

2666-8211/© 2022 The Author(s). Published by Elsevier B.V. This is an open access article under the CC BY-NC-ND license (<http://creativecommons.org/licenses/by-nc-nd/4.0/>).

systems. For this purpose, 93 AHA-IL molecular structures were modeled by DFT method, considering 8 different anion head groups (pyrrole, pyrazole, imidazole, 3/4-triazole, indole, indazole and benzimidazole) functionalized with 6 different substituents (H, CH<sub>3</sub>, CN, CF<sub>3</sub>, Br, S-CH<sub>3</sub>) located at distinct ring positions. Trihexyltetradecylphosphonium ([P<sub>66614</sub>]) was selected as common cation for all designed AHA-ILs, since phosphonium cations have been widely used as benchmark cations in previous studies due to their low costs and high thermal stability [15, 16, 19, 20, 25, 26]. The absorption isotherms of all studied CO<sub>2</sub>+AHA-IL systems were predicted by means of the recently reported DFT/COSMO-RS methodology [20], from calculated thermodynamic data (reaction enthalpy, entropy, Gibbs energy, reaction equilibria constant, and Henry's constant). The obtained thermochemical information was successfully incorporated in Aspen Plus commercial process simulator using COSMO-based/Aspen computational approach [23] to model 3 different industrial CO<sub>2</sub> capture processes using 12 representative AHA-ILs designed in this work. Absorption and regeneration stages using commercial packing columns were described by rigorous Rate-based simulations. A techno-economic analysis was performed using the selected AHA-ILs -presenting a representative CO<sub>2</sub>-IL reaction enthalpy range (from -30 to -64 kJ/mol)- for post-combustion, biogas, and pre-combustion systems. The CO<sub>2</sub> capture process performance was evaluated by means of chemicals and energy consumptions, equipment, and variable operating costs. A comparison to previous results obtained with benchmark AHA-ILs -or conventional absorption technology based on amine solutions- revealed the finding of new promising AHA-ILs for CO<sub>2</sub> capture to be synthesized and experimentally tested soon.

## 2. Computational methodology

### 2.1. Thermochemical data calculation of the CO<sub>2</sub>-IL reaction

The reaction enthalpy ( $\Delta H_R$ ), Gibbs energy ( $\Delta G_R$ ) and entropy ( $\Delta S_R$ ) of all possible AHA-ILs (see Table 1) were determined through vibrational frequency calculations after the optimization of the molecular geometries of the ILs and the reaction products, which were performed by Turbomole 7.4 software, following the computational and experimentally validated methodology described elsewhere [20]. All geometries were optimized using the B3-LYP DFT-functional paired with def2-TZVP basis set and DFT-D3 dispersion term, including COSMO solvation effect, whereas vibrational frequency calculations determined the electronic energy minimum. The partition function at 25°C and a scaling factor of 0.95 were considered when calculating absolute enthalpies and Gibbs energies of the molecules. Thereby, thermochemical data for the reactions were calculated as the difference between the sum of the contributions of the products and the reactants from DFT calculations [20]. Only the anion takes part in the 1:1 reaction mechanism because the binding to form the reaction product occurs between the molecule of CO<sub>2</sub> and the heterocyclic N of the anion [16, 19, 25]. All AHA-ILs share trihexyltetradecylphosphonium ([P<sub>66614</sub>]) cation, since it is generally argued to be chemically inert and thermally stable [16, 19] and only experimental data of [P<sub>66614</sub>]-based ILs was available in literature to validate the proposed methodology [19, 20]. Distinct heterocyclic N of the anion binding the CO<sub>2</sub> molecule was considered if possible. All the different conformers are grouped in 4 positioning types regarding on the substituent (R) location and the CO<sub>2</sub> binding site (N<sup>-</sup>) relative positions in Table 1: N-CR-C (Type I), N-CR-N (Type II), N-N-CR (Type III), and N-C-CR (Type IV).

**Table 1**  
Abbreviation and structure of the anions studied.

Name and Abbreviation	Base Anion	Bond N-CR-C (Type I)	Bond N-CR-N (Type II)	Bond N-N-CR (Type III)	Bond N-C-CR (Type IV)
Pyrrole [Pyr]			-	-	
Pyrazole [Pyra]			-		
Imidazole [Im]				-	
1,2,3-Triazole [3-Triaz]			-		
1,2,4-Triazole [4-Triaz]		-			-
2,3-Benzopyrrole or Indole [BnPyr]					
1,2-Benzopyrazole or Indazole [BnPyra]					
1,3-Benzimidazole [BnIm]					

## 2.2. Prediction of CO<sub>2</sub>+AHA-IL chemical absorption isotherms

A thermodynamic model successfully applied in previous works was used to predict the CO<sub>2</sub> absorption isotherms in AHA-ILs (Eq. (1)) by means of DFT/COSMO-RS calculations [20]. It combines both physical and chemical absorption using Henry's Law besides a traditional chemical equilibrium constant [13, 20, 23].

$$z = \frac{P_{CO_2}}{K_H - P_{CO_2}} + \frac{K_{eq} \cdot P_{CO_2} \cdot C}{K_H + K_{eq} \cdot P_{CO_2}} \quad (1)$$

where  $z$  is the molar ratio of CO<sub>2</sub> absorbed per mol of IL,  $P_{CO_2}$  is the CO<sub>2</sub> partial pressure in bar,  $K_H$  is the CO<sub>2</sub> Henry's law constant in the IL in bar,  $K_{eq}$  is the reaction equilibrium constant and  $C$  is an empirical ratio representing the AHA-IL available to react with the CO<sub>2</sub> molecule, whose value is fixed to 0.9 as reported in previous literature [25].

The CO<sub>2</sub> chemical absorption was represented by a 1:1 reversible reaction ( $IL + CO_2 \rightleftharpoons PROD$ ) in which the CO<sub>2</sub> molecule binds to the heterocyclic N of the anion to form the reaction product ( $PROD$ ) as demonstrated in literature [16, 19, 25]. Its chemical absorption equilibrium constant ( $K_{eq}$ ) can be estimated from DFT calculations at different temperatures by Van't Hoff equation (Eq. (2)) and implemented into Aspen Plus Reactive-Distillation equilibrium reaction using the temperature dependence parameters of its Arrhenius relationship (Eq. (3)).

$$\ln K_{eq} = \frac{\Delta S_R}{R} - \frac{\Delta H_R}{RT} \quad (2)$$

$$\ln K_{eq} = A + \frac{B}{T} \quad (3)$$

The CO<sub>2</sub> physical absorption was described by Henry's Law.  $K_H$  of CO<sub>2</sub> in AHA-ILs can be obtained from COSMO-RS calculations at different temperatures and included into Aspen Properties using the same Arrhenius equation (Eq. (4)).

$$\ln K_H = A + \frac{B}{T} \quad (4)$$

It requires defining CO<sub>2</sub> as a Henry component in Aspen Properties and generating by Turbomole the independent ions COSMO files at B-P86/TZVP level for COSMO-RS computations performed by COMOS-Therm 19 software. An experimental correction factor of 0.73, from comparison of COSMO-RS/experimental literature data of CO<sub>2</sub>  $K_H$  values in ILs, was applied to the predicted values that then needs to be included in Aspen Plus Henry's Law definition. Additional information about this method can be found in detail on our previous works [13, 20, 23]. The estimated CO<sub>2</sub> absorption isotherms can be found in Figure S1 of Supplementary Material.

## 2.3. Component definition and property method specification

Aspen Plus v11 commercial process simulator was used to model post-combustion, biogas, and pre-combustion CO<sub>2</sub> capture processes. Thus, all AHA-ILs considered need to be introduced as pseudo-components following the previously reported multiscale COSMO-based/Aspen Plus methodology [13, 23, 27]. The quantum chemical structure optimizations performed at B-P86/TZVP level together with COSMO-RS calculations of molecular weight, boiling point, density, molecular volume and the sigma-profile for all AHA-ILs and their reaction products were used to specify the COSMOSAC property method of the Aspen Plus simulations (in code 1, COSMOSAC method by Sandler et al. [28]). The experimental temperature dependent [P<sub>66614</sub>] [2-CNPy] viscosity data were incorporated to better describe the CO<sub>2</sub> mass transfer kinetics in the proposed AHA-ILs [13, 23]. Thermodynamic properties, chemical reaction and kinetic parameters used to define the CO<sub>2</sub>-ILs systems in Aspen Plus simulations are summarized in Table S1 of Supplementary Material.

## 2.4. CO<sub>2</sub> capture process design, simulation and cost estimation

Table 2 reports the inlet gas stream conditions for post-combustion, biogas, and pre-combustion processes, being its composition simplified to the two major constituents (CO<sub>2</sub> plus N<sub>2</sub>, CH<sub>4</sub> or H<sub>2</sub>).

The scheme of the ILs-based CO<sub>2</sub> capture process is depicted in Fig. 1, according to the previously designed flowsheet [13, 23]. In the absorption column (T-100), the gas stream to be treated (S-01 at Table 2 conditions) encounters the IL recirculated from the regeneration column at adiabatic operating conditions (S-07), with 90% of the CO<sub>2</sub> fed being absorbed. The CO<sub>2</sub> cleaned gas (S-02) gets out of the absorber through the top meanwhile in bottom the saturated absorbent stream (S-03) exits the tower to be pressurized (P-100) to reach the regeneration column (T-101), which operates at vacuum pressure (E-100 and C-100). There is not any preheating step, so a forced circulation (P-101) reboiler (E-101) heats the IL to achieve its regeneration. The CO<sub>2</sub> captured leaves the column after its desorption (S-08) and the IL regenerated (S-05) is pressurized (P-102) and cooled (E-102) before it is recirculated to the absorption column (T-100).

The CO<sub>2</sub> absorption (T-100 in Fig. 1) and IL regeneration (T-101 in Fig. 1) columns were modeled as packed columns using Aspen Plus's RADFRAC rigorous model. Rate-based mode calculations were performed to consider the CO<sub>2</sub> mass transfer kinetic process -10 computation stages for the absorber and 6 for the stripper- and Aspen Plus's Reactive-Distillation equilibrium reaction was employed to describe the chemical reaction between CO<sub>2</sub> and each IL, whose  $K_{eq}$  equation must be specified with the temperature dependence parameters (see Table S1 of Supplementary Material) explained before [13, 20, 23]. The reaction occurs in the liquid phase and the equilibrium constant basis is the mole fraction. Both columns consisted of a 15 m of packing height, using Flexipac 700Y structured packing for both Columns Internals, and the Interactive sizing tool calculated the suitable diameter to maintain a fractional capacity of 80% in all cases.

The absorber operates at the corresponding inlet stream total pressure depending on the treatment process (CO<sub>2</sub> partial pressures from 0.13 to 13 bar, see Table 2) and adiabatic operating conditions, achieving each system a 90% of CO<sub>2</sub> uptake. Regarding the IL regeneration unit, it operates at 100°C and 0.1 bar of vacuum pressure to prevent thermal decomposition [13, 23]. On the one hand, the forced circulation (P-101) reboiler (E-101) supplies the sensible heat for solvent heating, the latent heat for physically absorbed CO<sub>2</sub> vaporization and the reaction heat for chemically absorbed CO<sub>2</sub> desorption. On the other hand, the energy required for vacuum operation was estimated by Aspen Plus's isentropic compressor model (C-100), emulating the pressure drop from 1 to 0.1 bar directly to the vapor after cooling it to 35°C (E-100). The regenerated IL is then pressurized (P-102) and cooled down (E-102) to reach the top of the absorber at 40°C.

The discharge pressures of the circulation pumps (P-100 and P-102) were calculated using the pipeline model implemented as explained elsewhere [13], specifying outlet pressures and temperatures (S-03 stream conditions for P-100 and 100°C and S-07 pressure for P-102) and selecting Gear's model integration method and Beggs-Brill frictional and hold up correlations. The forced circulation reboiler pump (P-101) was only considered when estimating equipment costs. The pumps and vacuum compressor power demands were estimated using a

**Table 2**  
Inlet gas streams properties.

	Post-combustion	Biogas	Pre-combustion
Temperature (°C)	40	40	40
Pressure (bar)	1.0	3.2	32.7
CO <sub>2</sub> molar flow (kmol/h)	100	100	100
Composition (%mol)			
$x_{CO_2}$	13	38	40
$x_{N_2}$	87	—	—
$x_{CH_4}$	—	62	—
$x_{H_2}$	—	—	60

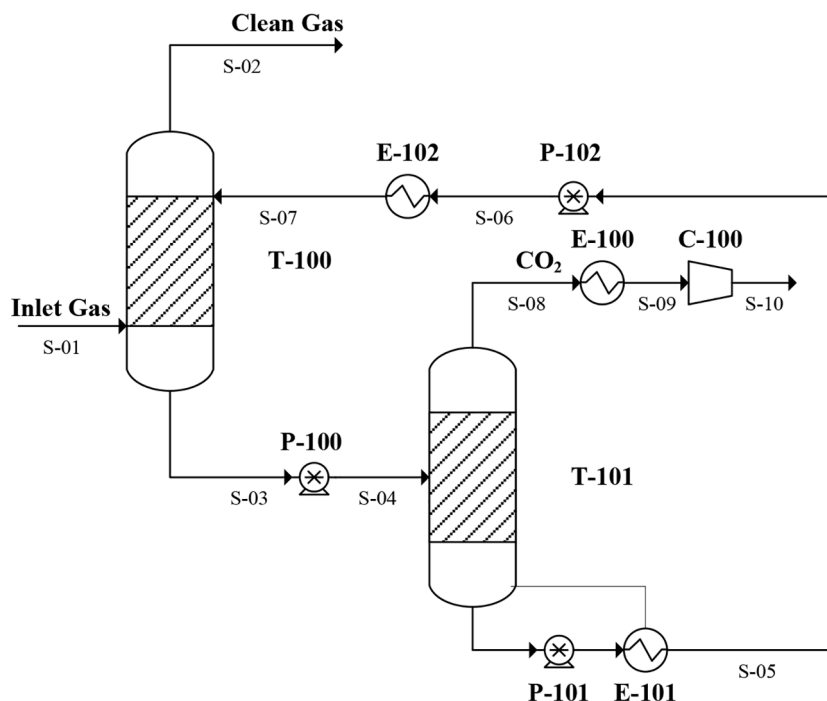


Fig. 1. ILs-based CO<sub>2</sub> chemical absorption process diagram.

pumping/compression efficiency of 60% and a driver efficiency of 85% according to heuristic rules [13, 29].

Since only equipment investment and utilities costs can be optimized through process engineering, they were picked to represent the capital and operating expenses in the economic analysis, respectively. Costing of all process equipment was accomplished via Aspen Process Economic Analyzer (APEA) v11 (2018 pricing basis) under the same aforementioned mapping assumptions [13]. The variable operating cost was calculated as the sum of the costs of the electricity consumed by the pumps (P-100, P-101 and P-102) and the vacuum compressor (C-100), the low-pressure steam required in the regeneration column reboiler (E-101) and the cooling water used as refrigerant in the vacuum unit (E-100) and in the cooler prior to the absorption column (E-102). Their default prices implemented given by Aspen Plus ( $7.75 \cdot 10^{-2}$  \$/kWh for electricity,  $1.90 \cdot 10^{-6}$  \$/kJ for LP steam and  $2.12 \cdot 10^{-7}$  \$/kJ for cooling water) and an operation time of 8000 h/year were assumed [13]. The detailed procedure for cost estimation can be found in a previous article [13]. The IL cost was not included due to the uncertainty about the large-scale production price nowadays and it is not worth considering when comparing hypothetical ILs.

### 3. Results

#### 3.1. Functional group effect on CO<sub>2</sub>-ILs thermochemistry

To address the molecular design of new absorbents, enthalpy ( $\Delta H_R$ ), Gibbs energy ( $\Delta G_R$ ) and entropy ( $T \cdot \Delta S_R$ ) of the reaction between CO<sub>2</sub> and AHA-ILs based on 8 representative anions with different N-heterocyclic rings and several substituents were analyzed. Table 3 shows DFT-calculated  $\Delta H_R$ ,  $\Delta G_R$ , and  $T \cdot \Delta S_R$  values for the 8 N-heterocyclic ring bases proposed.

The anions with a lower number of N in the ring generally have a more exothermic reaction with CO<sub>2</sub>, because more basic and smaller anions exhibit more prominent interactions with CO<sub>2</sub> [19]. Thus, anions reported in Table 3 could be classified in increasing order of reaction exothermicity as follows: [Pyr] > [BnPyr] > [Pyra] > [BnPyra] > [Im] > [BnIm] > [4-Triaz] > [3-Triaz]. Moreover, anions with more exothermic reactions are associated with a more negative Gibbs energy

Table 3

Thermochemical data of the AHA-IL reactions with CO<sub>2</sub> calculated with B3-LYP functional using COSMO solvation method at 25°C.

Base anion	$\Delta H_R$ (kJ/mol)	$\Delta G$ (kJ/mol)	$T \cdot \Delta S$ (kJ/mol)
[Pyr]	−88.44	−60.65	−27.79
[BnPyr]	−77.24	−50.09	−27.15
[Pyra]	−63.54	−36.20	−27.34
[BnPyra]	−59.92	−33.87	−26.06
[Im]	−59.76	−32.44	−27.32
[BnIm]	−50.94	−27.60	−23.34
[4-Triaz]	−34.41	−7.61	−26.80
[3-Triaz]	−24.75	−1.48	−23.27

value that indicates greater spontaneity. Current results confirm that the thermodynamics of CO<sub>2</sub>-IL reaction is governed by enthalpy, playing entropy a minor role with similar  $T \cdot \Delta S_R$  values for all systems. In addition, the effect of the substituent and its position in the heterocyclic ring

Table 4

$\Delta H_R$  values of CO<sub>2</sub>+AHA-IL reaction for functionalized anions depending on the substituent nature and ring position (Types I-IV).

Bond type	Base	CN	CF <sub>3</sub>	Br	S-CH <sub>3</sub>	CH <sub>3</sub>
I	[3-Triaz]	17.1	14.2	8.6	−18.6	−27.8
	[Im]	−16.5	−15.9	−20.9	−38.3	−57.8
	[Pyr]	−41.9	−40.2	−42.7	−65.7	−84.3
	[Pyra]	−18.9	−17.9	−22.5	−38.0	−63.7
II	[4-Triaz] <sup>a</sup>	12.1	11.5	3.7	−22.5	−31.9
	[4-Triaz] <sup>b</sup>	8.0	6.7	−0.8	−31.1	−35.5
	[Im]	−14.6	−14.7	−21.3	−37.6	−61.2
	[Pyra]	−29.8	−41.1	−55.9	−58.5	−76.7
III	[3-Triaz]	7.5	−4.6	−11.4	−22.6	−33.7
	[4-Triaz]	−4.5	−14.9	−19.6	−31.7	−41.7
	[Pyra]	−29.8	−41.1	−55.9	−58.5	−76.7
	[3-Triaz]	3.8	−5.3	−11.2	−21.4	−30.7
IV	[Im]	−27.8	−39.1	−44.1	−51.7	−65.8
	[Pyr]	−53.6	−64.0	−72.6	−76.9	−95.5
	[Pyra]	−30.1	−41.1	−49.3	−52.5	−68.1
	[BnPyr]	−59.9	−66.2	−70.1	−75.2	−80.1
	[BnPyra]	−43.6	−51.4	−52.9	−56.3	−62.5
	[BnIm]	−35.1	−40.3	−43.7	−43.8	−55.6

with respect to the N atom binding the CO<sub>2</sub> molecule (Types I, II, III and IV) in the CO<sub>2</sub>-IL reaction enthalpy (Table 4) and Gibbs energy (Table S2 of Supplementary Material) were analyzed for a total of 85 AHA-ILs.

A remarkably wide range of CO<sub>2</sub>-IL reactivity behavior was found depending on the anion structure, evolving from strongly exothermic (−96 kJ/mol) to slightly endothermic (17 kJ/mol) reactions (see Figure S2 of Supplementary Material) as displayed in Table 4. Fig. 2 shows the effect of each substituent at each position on the ring (see Table 1) on the CO<sub>2</sub>-IL reaction enthalpy, represented as the average difference in  $\Delta H_R$  values for [Pyr], [Pyr], [Im], [3-Triaz] and [4-Triaz] based anions with ( $\Delta H_R$  values of Table 4) and without ( $\Delta H_R$  values of Table 3) functionalization (the obtained difference in  $\Delta H_R$  values are collected in Table S3 of Supplementary Material along with  $\Delta G_R$  data in Table S4):

$$\Delta H_R \text{ Average Diff.} = \frac{\sum(\Delta H_R \text{ functionalized}) - (\Delta H_R \text{ nonfunctionalized})}{N^{\circ} \text{ of possible anions}} \quad (5)$$

The substituent effect is similar for the different head group anions. CH<sub>3</sub> group hardly varied the reaction enthalpy when it is next to N-CO<sub>2</sub> bond (Types I and II) and even reduced it (more exothermic reaction) when it is separated by a N or C (Types III and IV). The rest of substituents showed the opposite effect, decreasing the exothermicity of the CO<sub>2</sub>-IL reaction in the following order: CH<sub>3</sub> < S-CH<sub>3</sub> < Br < CF<sub>3</sub> < CN. Regarding the influence of the substituent location on heterocyclic ring, a stronger effect was observed when the substituent is next to the N to which CO<sub>2</sub> binds (Types I and II) than if an atom is found between them, either N or C (Types III and IV). It was demonstrated to be caused by a combination of inductive,  $\pi$  conjugation, and steric effects for cyano-substituted pyrrolidines [16]. Current results demonstrate that it is possible to tailor the CO<sub>2</sub>-IL reaction thermochemistry -by combining substituent type/location and heterocyclic anion ring- in order to design optimal chemical absorbents for CO<sub>2</sub> capture.

### 3.2. Technical analysis

A total of 12 AHA-ILs presenting a wide range of enthalpies of reaction (from −30.1 to −63.5 kJ/mol) were evaluated in post-combustion, biogas and pre-combustion CO<sub>2</sub> capture processes using Aspen Plus to analyze how the heat of reaction affects solvent and energy requirements besides equipment and utilities costs. Fig. 3 illustrates the

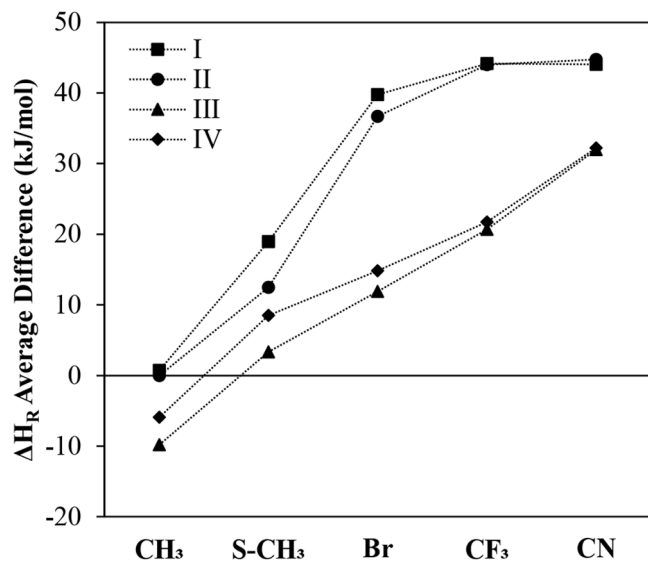


Fig. 2. Average reaction enthalpy difference [ $\Delta H_R$  (functionalized anion) -  $\Delta H_R$  (non-functionalized anion)] depending on the substituent group and its position (Types I-IV) in the heterocyclic ring.

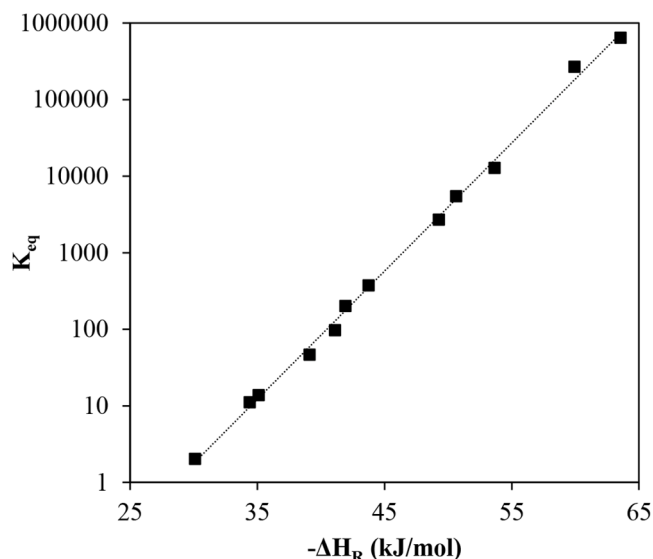


Fig. 3. Enthalpy of reaction ( $\Delta H_R$ ) vs. equilibrium constant ( $K_{eq}$ ) for the 12 CO<sub>2</sub>-ILs systems at 40°C.

relationship between the reaction equilibrium constant ( $K_{eq}$ ) and the reaction enthalpy ( $\Delta H_R$ ) for the 12 CO<sub>2</sub>-IL selected systems at 40°C.

Fig. 3 exhibits the linear relationship between  $K_{eq}$  and  $\Delta H_R$  values for CO<sub>2</sub>-IL reactions as demonstrated elsewhere [23], ranging a remarkably wide of reaction behavior (from reversible to nearly irreversible) in which higher  $K_{eq}$  values imply greater absorption capacities at lower CO<sub>2</sub> partial pressure. Therefore, noticeable different absorption isotherms for the 12 selected AHA-ILs (see Figure S1 of Supplementary Material) were obtained. Table 5 collects the reaction enthalpy of the 12 CO<sub>2</sub>-IL systems, chemical ( $K_{eq}$ ) and physical ( $K_H$ ) equilibrium constants together with some relevant properties of these AHA-ILs. As we noted, a wide range of CO<sub>2</sub> chemical absorption capacities were obtained in terms of  $K_{eq}$ ; in contrast, the close  $K_H$  values indicate similar CO<sub>2</sub>

Table 5

Aspen Plus estimated physical properties, CO<sub>2</sub>-ILs Henry's law constant ( $K_H$ ), reaction equilibrium ( $K_{eq}$ ) constant and enthalpy of reaction ( $\Delta H_R$ ) at 40°C for 12 AHA-ILs, calculated using DFT/COSMO/Aspen approach.

Ionic liquid	$\Delta H_R$ (kJ/mol)	$K_{eq}$	$K_H$ (bar)	MW (g/mol)	$\rho$ (g/cm <sup>3</sup> )	$C_p$ (kJ/kg·K <sup>-1</sup> )
[P <sub>66614</sub> ] [Pyr]	−63.5	644,807.7	34.9	550.9	0.88	2.14
[P <sub>66614</sub> ] [BnPyra]	−59.9	269,226.3	32.2	601.0	0.91	2.06
[P <sub>66614</sub> ][3- CNPyra]	−53.6	12,814.7	31.1	574.9	0.89	2.10
[P <sub>66614</sub> ] [BnIm]	−50.6	5491.3	32.3	601.0	0.91	2.05
[P <sub>66614</sub> ][4- BrPyra]	−49.3	2694.4	23.1	629.8	0.98	1.89
[P <sub>66614</sub> ][6- BrBnIm]	−43.7	374.3	29.7	679.9	1.00	1.75
[P <sub>66614</sub> ][2- CNPyra]	−41.9	201.5	30.9	574.9	0.89	2.12
[P <sub>66614</sub> ][3- CF <sub>3</sub> Pyra]	−41.1	96.9	33.7	618.9	0.94	1.94
[P <sub>66614</sub> ][4- CF <sub>3</sub> Im]	−39.1	46.6	27.2	618.9	0.93	2.00
[P <sub>66614</sub> ][6- CNBnIm]	−35.1	13.8	29.3	626.0	0.92	1.95
[P <sub>66614</sub> ][4- Triaz]	−34.4	11.1	32.7	551.9	0.89	2.12
[P <sub>66614</sub> ][4- CNPyra]	−30.1	2.0	30.4	575.9	0.90	2.06



physical absorption in the selected AHA-ILs, in good agreement with previous conclusions [16, 19].

Attending to the techno-economic evaluation, solvent and energy demands of the CO<sub>2</sub> capture process, (Fig. 1) calculated by Aspen Plus simulations for the 12 AHA-ILs proposed, were analyzed. Fig. 4 represents both IL flow rate and total energy consumption depending on CO<sub>2</sub>-IL  $\Delta H_R$  value for post-combustion (a), biogas (b) and pre-combustion (c) processes, which achieve 90% of CO<sub>2</sub> uptake from inlet gas streams of Table 2.

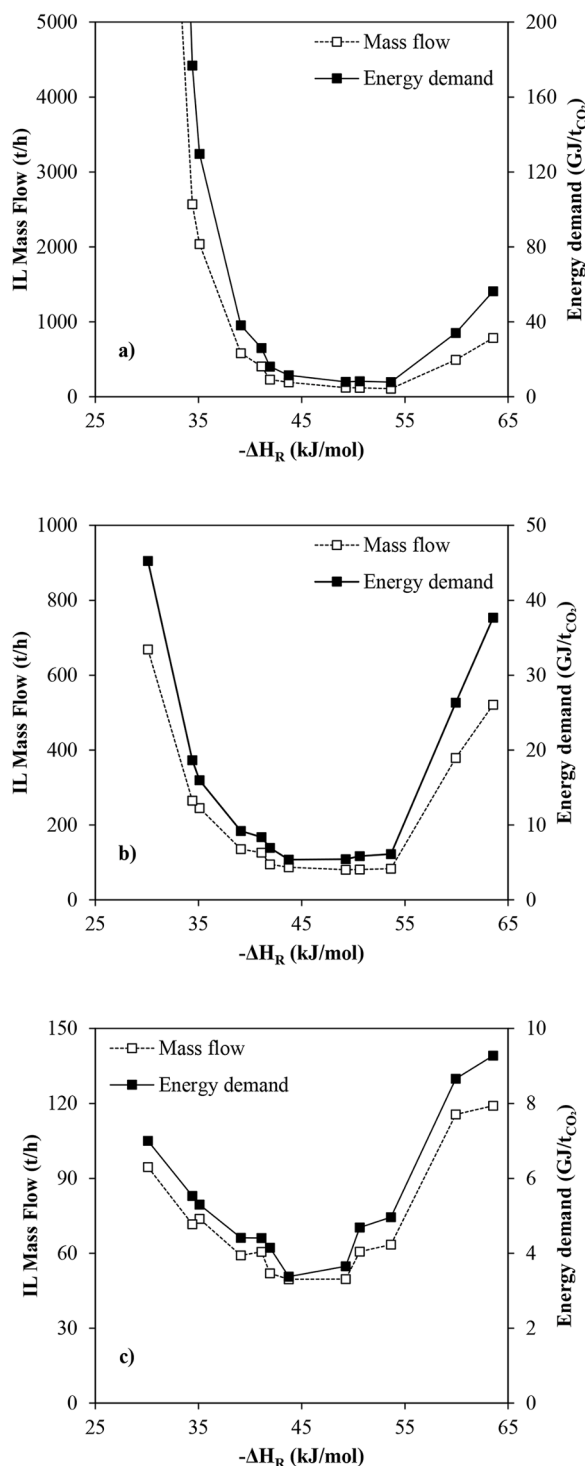


Fig. 4. IL mass flow and total energy required depending on the CO<sub>2</sub>-IL reaction enthalpy for post-combustion (a), biogas (b) and pre-combustion (c) CO<sub>2</sub> capture processes.

As can be seen in Fig. 4, solvent and energy requirements for CO<sub>2</sub> capture process follow a similar trend, obtaining clear minimum values in the studied range of reaction enthalpies for all post-combustion, biogas and pre-combustion systems. This fact is related to two combined effects. On the one hand, increasing reaction exothermicity means not only higher CO<sub>2</sub> absorption capacity, and consequently lower IL flow requirement, but also higher temperature on the absorber, which improves mass transfer rate by reducing the IL viscosity and declines the heating duty on the reboiler owing to a warmed-up IL [13, 23]. On the other hand, since more exothermic CO<sub>2</sub>-IL reactions are harder to reverse, the efficiency of regeneration stage is reduced, increasing IL and energy demands [30]. As a result, optimum performances were obtained in the reaction enthalpy range between  $-43$  and  $-54$  kJ/mol, very similar to those reported in literature studies (optimum around  $-49$  kJ/mol) [22, 24]. This range widens the variety of possibilities when synthesizing new suitable AHA-ILs for these CO<sub>2</sub> capture systems, being able to select those presenting the most suitable enthalpy according to the operating conditions. Solvent and energy requirements are reduced as the CO<sub>2</sub> partial pressure increases (moving from 0.13 on post-combustion to 3.8 on biogas and 13 bar on pre-combustion), together with a clear IL flow rate domain over the total energy demand in all cases, in accordance with previous results [13, 23]. The optimal  $\Delta H_R$  values in Fig. 4 indicates that slightly less exothermic reaction is advantageous when CO<sub>2</sub> partial pressure increases (post-combustion:  $-53.6$  kJ/mol; biogas:  $-49.3$  kJ/mol; pre-combustion:  $-43.7$  kJ/mol).

Table 6 compares the process performance of [P<sub>66614</sub>][2-CNPy] ( $-41.9$  kJ/mol of  $\Delta H_R$  value), as benchmark AHA-IL used in previous studies [13, 16, 19, 23, 31, 32] to that of [P<sub>66614</sub>][4-BrPyra] ( $-49.3$  kJ/mol of  $\Delta H_R$  value), a non-synthesized AHA-IL with enhanced behavior in all studied CO<sub>2</sub> capture systems (post-combustion, biogas and pre-combustion). Absorbent molar flow rate, columns' dimensions, electric demand, cooling requirement and reboiler duty -divided into its three main contributions at different operating conditions- are collected in Table 6.

As shown in Table 6, the estimated mass flow rates using the new [P<sub>66614</sub>][4-BrPyra] absorbent are remarkably lower than those needed using the benchmark AHA-IL, particularly at lower CO<sub>2</sub> partial pressure (post-combustion: 47%; biogas: 15%; pre-combustion: 4%). In fact, [P<sub>66614</sub>][4-BrPyra] achieved the minimum flow rates on biogas and pre-combustion systems, although on post-combustion CO<sub>2</sub> capture [P<sub>66614</sub>][3-CNPy] ( $-53.6$  kJ/mol of  $\Delta H_R$  value) was the best AHA-IL, needing only 108.5 t/h. This demonstrates that molecular design can be successfully applied to improve solvent performance.

Comparing the energy demands, [P<sub>66614</sub>][4-BrPyra]-based CO<sub>2</sub> capture processes consumes less thermal energy than those using [P<sub>66614</sub>][2-CNPy] (post-combustion: 51%; biogas: 24%; pre-

Table 6

Summary of solvent, energy and equipment sizing requirements for CO<sub>2</sub> capture process using [P<sub>66614</sub>][2-CNPy] and [P<sub>66614</sub>][4-BrPyra] absorbents, calculated in this work using DFT/COSMO/Aspen approach.

Ionic liquid System	[P <sub>66614</sub> ][2-CNPy]			[P <sub>66614</sub> ][4-BrPyra]		
	Post-C	Biogas	Pre-C	Post-C	Biogas	Pre-C
IL flow rate (t/h)	229.4	94.8	51.9	122.1	80.5	49.6
Cyclic capacity (mol/kg)	0.39	0.95	1.73	0.74	1.12	1.81
Electricity (GJ/tCO <sub>2</sub> )	0.4	0.4	0.4	0.4	0.4	0.4
Cooling duty (GJ/tCO <sub>2</sub> )	7.9	3.3	1.9	3.8	2.5	1.6
Reboiler duty (GJ/tCO <sub>2</sub> )	7.8	3.3	1.8	3.8	2.5	1.6
Sensible heat	6.5	2.0	0.7	2.2	0.9	0.3
Reaction heat	0.9	0.9	0.7	1.1	1.1	0.8
Latent heat	0.4	0.4	0.4	0.5	0.5	0.5
Abs. column dimensions (m)	H 15.0	15.0	15.0	15.0	15.0	15.0
Reg. column dimensions (m)	D 3.2	1.7	1.1	2.8	1.6	1.1
Reg. column dimensions (m)	H 15.0	15.0	15.0	15.0	15.0	15.0
Reg. column dimensions (m)	D 2.6	1.9	1.6	2.1	1.8	1.7

combustion: 16%), even  $[P_{66614}][3\text{-CNPyr}]$  and  $[P_{66614}][6\text{-BrBnIm}]$  ( $-43.7$  kJ/mol of  $\Delta H_R$  value) minimize the global energy demand 0.2 GJ/tCO<sub>2</sub> below  $[P_{66614}][4\text{-BrPyra}]$  values. Nevertheless, the heating necessity to regenerate  $[P_{66614}][4\text{-BrPyra}]$  does not exceed in any case that required by MEA-based processes (4.2 GJ/tCO<sub>2</sub> on post-combustion [33], 4.5 GJ/tCO<sub>2</sub> on natural gas [34] or 3.0 GJ/tCO<sub>2</sub> on pre-combustion [9]). The contribution of each energy part can be analyzed attending to Table 6. The electricity power consumption is equal at different CO<sub>2</sub> partial pressure since the compression requirement is the same ( $\approx 0.35$  GJ/tCO<sub>2</sub>) and the higher pressure on biogas and pre-combustion compensates the higher flow rate to be pumped on post-combustion [13]. Table 6 confirms the flow rate dependence of the heat exchangers duties involving the IL, since duties are drastically reduced when less IL is needed [13]. Attending to the reboiler, there is a significant contribution of the sensible heat ( $\geq 21\%$ ) to the total thermal necessities in all cases. Compared to the heat for chemically absorbed CO<sub>2</sub> desorption (1.1 GJ/tCO<sub>2</sub>, 29%), solvent heating is the major requirement on post-combustion CO<sub>2</sub> capture (2.2 GJ/tCO<sub>2</sub>, 58%). However, sensible heat decreases 59% (0.9 GJ/tCO<sub>2</sub>) on biogas and 86% (0.3 GJ/tCO<sub>2</sub>) on pre-combustion cases referring to  $[P_{66614}][4\text{-BrPyra}]$  data of Table 6, where less IL has to be heated, allowing a more efficient energy consumption in the reboiler focused on reversing the CO<sub>2</sub>-IL reaction. In fact, the increase of the physically absorbed CO<sub>2</sub> at high pressure entails less amount of reaction product to achieve 90% of CO<sub>2</sub> capture. Then, the energy demand to recover the CO<sub>2</sub> and regenerate the IL solvent is reduced (1.1 vs. 0.8 GJ/tCO<sub>2</sub>). Finally, the column sizes for absorption and regeneration operations are in the standard industrial ratios ( $5 < H/D < 30$ ) [29] for all studied CO<sub>2</sub> capture systems using  $[P_{66614}][4\text{-BrPyra}]$ , larger equipment volumes being necessary when increasing the absorbent flow rate. In summary, current results demonstrate that it is possible to improve the CO<sub>2</sub> capture process efficiency by conveniently tuning CO<sub>2</sub>-IL reaction enthalpy through molecular design.

The reported effect of the CO<sub>2</sub>-IL reaction enthalpy on the solvent performance can be easily understood attending to the absorber inlet (S-07) and outlet (S-03) CO<sub>2</sub> loading capacities whose difference is the cyclic capacity of the IL (also named gap capacity in previous works [13, 23]), represented in Fig. 5. The cyclic capacity values (mol/kg) achieved using  $[P_{66614}][2\text{-CNPyr}]$  and  $[P_{66614}][4\text{-BrPyra}]$  were also presented in Table 6.

Fig. 5a shows a coincidence between the minimum solvent and energy consumption and the maximum cyclic capacity [13, 23] in the range from  $-43$  to  $-54$  kJ/mol reaction enthalpy values. Those AHA-ILs, as  $[P_{66614}][4\text{-BrPyra}]$ , getting higher cyclic capacity exhibited

lower solvent and energy consumptions. In addition, it can be observed a cyclic capacity increase with CO<sub>2</sub> partial pressure (biogas and pre-combustion systems) due to an improved CO<sub>2</sub> absorption. Trends of Fig. 5a can be explained by analyzing rich and lean IL loading capacities shown in Fig. 5b. Although less exothermic reactions than  $-41$  kJ/mol facilitate the IL regeneration leading to a solvent stream (S-07 in Fig. 1) with lower CO<sub>2</sub> loading, the CO<sub>2</sub> chemically absorbed is scarce (S-03 loading is poor), so low cyclic capacities were reached. On the contrary, more exothermic reactions than  $-54$  kJ/mol in which the chemical capture of CO<sub>2</sub> was highly favored but hard to reverse, worsened cyclic capacity values. These combined effects implied a maximum of cyclic capacity in the enthalpy range from  $-43$  to  $-54$  kJ/mol. Attending to Fig. 5, as CO<sub>2</sub> partial pressure increases the IL absorbs a larger amount of CO<sub>2</sub>, increasing the difference between inlet and outlet loading capacities and thus cyclic capacity. These results indicate a great process optimization margin by selecting proper operating conditions, getting a similar cyclic capacity but entailing a noticeable energy consumption decline.

### 3.3. Economic analysis

Fig. 6 reports the estimated operating and equipment costs for all studied CO<sub>2</sub> capture processes using the 12 selected AHA-ILs presenting different reactivity with CO<sub>2</sub>. Both expenses follow the energy and solvent consumptions trends of Fig. 4, in line with previous works [13]. Thus, minimum costs were obtained for the same range of reaction enthalpy values between  $-43$  and  $-54$  kJ/mol corresponding to suitable cyclic capacities values. Therefore, optimizing the IL cyclic capacity by tailoring its enthalpy of reaction with CO<sub>2</sub> reduced both equipment and utilities costs.

At post-combustion operating conditions the lowest operating cost achieved was 0.50 M\$/year using  $[P_{66614}][3\text{-CNPyr}]$ , very close to that 0.51 M\$/year obtained with  $[P_{66614}][4\text{-BrPyra}]$ , meanwhile biogas and pre-combustion systems presented 0.42 and 0.41 M\$/year with  $[P_{66614}][4\text{-BrPyra}]$  respectively, describing more cost-effective CO<sub>2</sub> capture processes than  $[P_{66614}][2\text{-CNPyr}]$  benchmark absorbent (0.80 – 0.43 M\$/year).

Regarding the equipment cost calculated using APEA, minimums are also located between  $-43$  and  $-54$  kJ/mol  $\Delta H_R$  range, since the IL volume rate brings the size of operating units. At low CO<sub>2</sub> partial pressure (post-combustion) greater cost differences associated with the variation of AHA-IL quantity can be noticed again. Here the 4.2 M\$ minimum equipment cost was obtained for  $[P_{66614}][4\text{-BrPyra}]$  versus

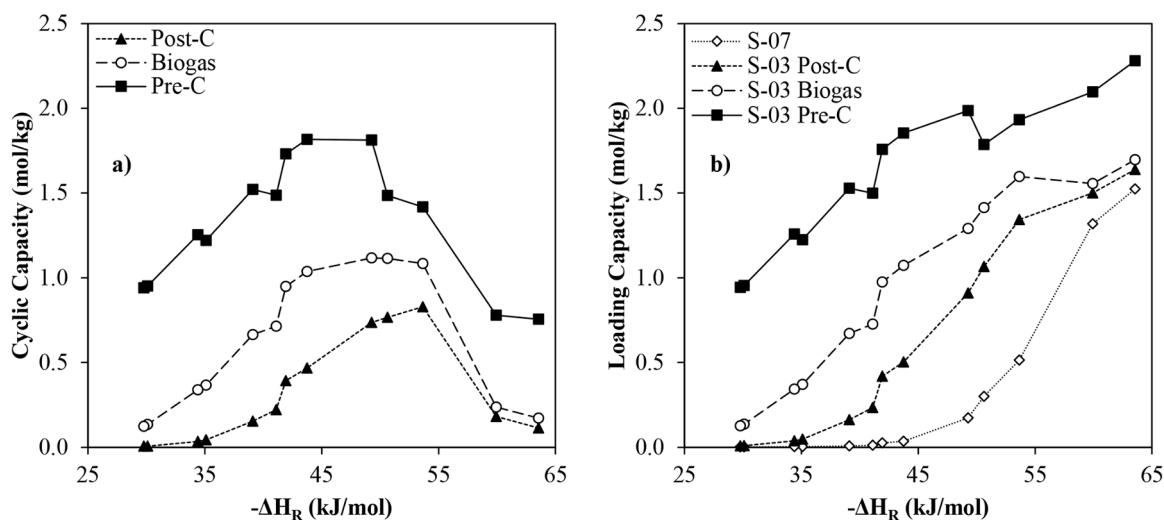


Fig. 5. IL cyclic capacity (a) and CO<sub>2</sub> loadings in rich (S-03) and lean (S-07) AHA-IL streams (b) at post-combustion, biogas and pre-combustion operating conditions depending on the CO<sub>2</sub>-IL reaction enthalpy.

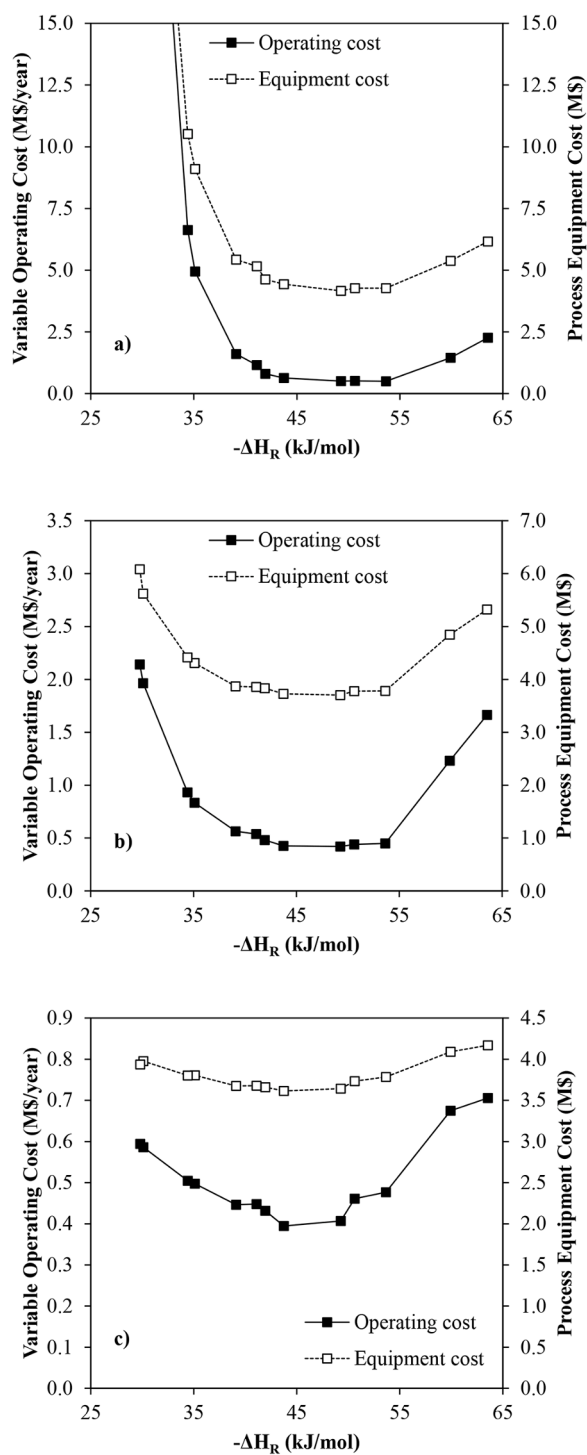


Fig. 6. Variable operating cost and equipment cost depending on the enthalpy of reaction for post-combustion (a), biogas (b) and pre-combustion (c)  $\text{CO}_2$  capture processes.

4.3 M\$ of  $[\text{P}_{66614}][3\text{-CNPy}]$ , whereas this investment value for  $[\text{P}_{66614}][2\text{-CNPy}]$  was 4.6 M\$. However, as pressure increases (from biogas to pre-combustion), these differences in the equipment cost are closer owing to a less drastic contrast between IL flow rates values and the vacuum compressor, which represents  $a \geq 70\%$  of the total investment on pre-combustion ( $\approx 3.0$  M\$) [13]. The minimum equipment cost on biogas (3.7 M\$) and on pre-combustion (3.6 M\$) was achieved using  $[\text{P}_{66614}][4\text{-BrPy}]$ , slightly lower compared to 3.8 M\$ and 3.7 M\$ corresponding values of  $[\text{P}_{66614}][2\text{-CNPy}]$ . Indeed, these resulting costs

could be improved by optimizing the operating conditions such as eliminating vacuum, which would reduce capital and operating costs, according to previous evidence [13, 14].

Other solvent properties such as molecular weight (MW), density ( $\rho$ ) or heat capacity ( $C_p$ ) have to be considered. Table 5 shows that molecular weight, density and heat capacity are slightly different depending on the AHA-IL structure, although their impact on the IL performance was found to be less significant compared to the reaction enthalpy. There are only few cases in which these properties became determinant. For example, the higher molecular weight value of  $[\text{P}_{66614}][4\text{-BrPy}]$  compared to  $[\text{P}_{66614}][\text{BnIm}]$  (see Table 5) equalized the mass flow on biogas system. It also happened in pre-combustion between  $[\text{P}_{66614}][4\text{-BrPy}]$  and  $[\text{P}_{66614}][6\text{-BrBnIm}]$ , the latter having a lower molar flow rate. Otherwise, the higher density of  $[\text{P}_{66614}][4\text{-BrPy}]$  (see Table 5) declined the volumetric flow of IL inside both columns compared to  $[\text{P}_{66614}][3\text{-CNPy}]$ , which reduced diameters and hence purchased cost discussed above. In addition, the lower  $C_p$  of  $[\text{P}_{66614}][6\text{-BrBnIm}]$  compared to  $[\text{P}_{66614}][4\text{-BrPy}]$  (see Table 5) decreased the energy requirement on pre-combustion case by descending heat exchangers duties, which meant fewer operating costs (0.40 vs. 0.41 M\$/year).

Thermal and chemical AHA-IL stabilities, environmental concerns or solvent costs are other relevant properties to be considered for selecting the best  $\text{CO}_2$  absorbent among those promising AHA-ILs studied in this work (reaction enthalpy from  $-43$  to  $-54$  kJ/mol in Figs. 4 and 6). In fact, current simulations were performed using the viscosity data of  $[\text{P}_{66614}][2\text{-CNPy}]$  with all AHA-ILs. The viscosity of other pyrazole-based AHA-ILs, such as  $[\text{P}_{66614}][3\text{-CF}_3\text{Py}]$  and  $[\text{P}_{66614}][3\text{-CF}_3\text{-5-CF}_3\text{Py}]$ , have been measured experimentally and their values (120 and 187 cP at  $40^\circ\text{C}$ , respectively) do not differ much from those of  $[\text{P}_{66614}][2\text{-CNPy}]$  (166 cP at  $40^\circ\text{C}$ ) [19], so an excessive extra kinetic limitation is not expected for  $[\text{P}_{66614}][4\text{-BrPy}]$  although it must be confirmed experimentally. On the other hand, it should be pointed that all results here reported were obtained computationally from DFT/COSMO-RS and Aspen Plus calculations, which have been demonstrated very useful for the early stages of conceptual design [13, 14, 20, 23, 35], but it requires experimental validation [23], since absorbent and energy consumptions of this work are deviated  $\approx 10\text{--}28\%$  compared to previous simulation results for identical  $\text{CO}_2$  capture processes using experimental  $\text{CO}_2$ - $[\text{P}_{66614}][2\text{-CNPy}]$  absorption isotherms (see Table S5 of Supplementary Material) [13].

#### 4. Conclusions

Combined DFT and COSMO-RS quantum chemical calculations were successfully applied to design AHA-ILs covering a wide range of reaction enthalpy values. Functionalizing  $[\text{Pyr}]$ ,  $[\text{BnPy}]$ ,  $[\text{Py}]$ ,  $[\text{BnPy}]$ ,  $[\text{Im}]$ ,  $[\text{BnIm}]$ ,  $[\text{4-Triaz}]$  and  $[\text{3-Triaz}]$  with  $\text{CN}$ ,  $\text{CF}_3$ ,  $\text{Br}$ ,  $\text{S-CH}_3$  and  $\text{CH}_3$  in different positions on each heterocyclic ring was analyzed. More basic and smaller anions were confirmed to achieve more exothermic reactions with  $\text{CO}_2$ .  $\text{CH}_3$ - group was found to be the substituent that least affects the enthalpy of reaction, but it could rise the exothermicity when it was further away from the  $\text{N-CO}_2$  bond. On the contrary, the  $\text{CN}$  group increases the enthalpy by 32 – 45 kJ/mol on average. Rate-based simulations of an adiabatic absorption column plus an IL regeneration at vacuum pressure were carried out to assess the performance of 12 representative AHA-ILs (having an enthalpy value from  $-30.1$  to  $-63.5$  kJ/mol) on post-combustion, biogas and pre-combustion  $\text{CO}_2$  chemical capture processes following the multiscale COSMO-based/Aspen Plus methodology. Tuning the enthalpy of reaction allowed the cyclic capacity optimization for new AHA-ILs at the cited operating conditions. An optimal range of  $\text{CO}_2$ -IL reaction enthalpy values from  $-43$  to  $-54$  kJ/mol minimized both solvent and energy requirements and, thus equipment and operating costs regardless of operating conditions. Multiple AHA-ILs presenting an enthalpy of reaction with  $\text{CO}_2$  in this range were designed; opening the opportunity of using other relevant criteria to select new competitive  $\text{CO}_2$  chemical absorbents.  $[\text{P}_{66614}][4\text{-}$



BrPyr) [−49.3 kJ/mol] reduced absorbent and global energy demands as well as equipment and operating costs compared to the benchmark [P<sub>66614</sub>][2-CNPy], consolidating as a new promising AHA-IL for CO<sub>2</sub> capture. Therefore, current study -linking molecular and processes scales- definitively contributes to address the experimental research of new CO<sub>2</sub> capture technology based on ILs. Future works will be focused on synthesizing these new AHA-ILs and characterizing their physical properties, thermal stability and CO<sub>2</sub> absorption isotherms, in order to advance in developing new more efficient and cost-effective CO<sub>2</sub> capture technology.

### Declaration of Competing Interest

The authors declare that they have no known competing financial interests or personal relationships that could have appeared to influence the work reported in this paper. The authors declare the following financial interests/personal relationships which may be considered as potential competing interests.

### Acknowledgments

The authors are grateful to Ministerio de Ciencia e Innovación of Spain (project PID2020–118259RB-I00) and Comunidad de Madrid (project P2018/EMT4348) for financial support and Centro de Computación Científica de la Universidad Autónoma de Madrid for computational facilities.

### Supplementary materials

Supplementary material associated with this article can be found, in the online version, at [doi:10.1016/j.cej.2022.100291](https://doi.org/10.1016/j.cej.2022.100291).

### References

- [1] L. Lombardi, G. Francini, Techno-economic and environmental assessment of the main biogas upgrading technologies, *Renew. Energy* 156 (2020) 440–458.
- [2] C. Antonini, K. Treyer, A. Streb, M. van der Spek, C. Bauer, M. Mazzotti, Hydrogen production from natural gas and biomethane with carbon capture and storage – a techno-environmental analysis, *Sustain. Energy Fuels* 4 (2020) 2967–2986.
- [3] M. Bui, C.S. Adjiman, A. Bardow, E.J. Anthony, A. Boston, S. Brown, P.S. Fennell, S. Fuss, A. Galindo, L.A. Hackett, J.P. Hallett, H.J. Herzog, G. Jackson, J. Kemper, S. Krevor, G.C. Maitland, M. Matuszewski, I.S. Metcalfe, C. Petit, G. Puxty, J. Reimer, D.M. Reiner, E.S. Rubin, S.A. Scott, N. Shah, B. Smit, J.P.M. Trusler, P. Webley, J. Wilcox, N. Mac Dowell, Carbon capture and storage (CCS): the way forward, *Energy Environ. Sci.* 11 (2018) 1062–1176.
- [4] W. Gao, S. Liang, R. Wang, Q. Jiang, Y. Zhang, Q. Zheng, B. Xie, C.Y. Toe, X. Zhu, J. Wang, L. Huang, Y. Gao, Z. Wang, C. Jo, Q. Wang, L. Wang, Y. Liu, B. Louis, J. Scott, A.-C. Roger, R. Amal, H. He, S.-E. Park, Industrial carbon dioxide capture and utilization: state of the art and future challenges, *Chem. Soc. Rev.* 49 (2020) 8584–8686.
- [5] F. Vega, F.M. Baena-Moreno, L.M. Gallego Fernández, E. Portillo, B. Navarrete, Z. Zhang, Current status of CO<sub>2</sub> chemical absorption research applied to CCS: towards full deployment at industrial scale, *Appl. Energy* 260 (2020), 114313.
- [6] S.E. Zanco, J.-F. Pérez-Calvo, A. Gasós, B. Cordiano, V. Becattini, M. Mazzotti, Postcombustion CO<sub>2</sub> capture: a comparative techno-economic assessment of three technologies using a solvent, an adsorbent, and a membrane, *ACS Eng. Au* 1 (2021) 50–72.
- [7] M.T. Mota-Martinez, J.P. Hallett, N. Mac Dowell, Solvent selection and design for CO<sub>2</sub> capture - how we might have been missing the point, *Sustain. Energy Fuels* 1 (2017) 2078–2090.
- [8] M.T. Mota-Martinez, P. Brandl, J.P. Hallett, N. Mac Dowell, Challenges and for the utilisation of ionic liquids as solvents for CO<sub>2</sub> capture, *Mol. Syst. Des. Eng.* 3 (2018) 560–571.
- [9] S. Valiani, N. Tahouni, M.H. Panjeshahi, Optimization of pre-combustion capture for thermal power plants using Pinch analysis, *Energy* 119 (2017) 950–960.
- [10] F. Ortlöf, M. Roschitz, M. Ahrens, F. Graf, T. Schubert, T. Kolb, Characterization of functionalized ionic liquids for a new quasi-isothermal chemical biogas upgrading process, *Sep. Purif. Technol.* 195 (2018) 413–430.
- [11] C.J. Clarke, W.-C. Tu, O. Levers, A. Bröhl, J.P. Hallett, Green and sustainable solvents in chemical processes, *Chem. Rev.* 118 (2018) 747–800.
- [12] R.F. Zheng, D. Barpaga, P.M. Mathias, D. Malhotra, P.K. Koech, Y. Jiang, M. Bhakta, M. Lail, A.V. Rayer, G.A. Whyatt, C.J. Freeman, A.J. Zwoster, K. K. Weitz, D.J. Heldebrant, A single-component water-lean post-combustion CO<sub>2</sub> capture solvent with exceptionally low operational heat and total costs of capture – comprehensive experimental and theoretical evaluation, *Energy Environ. Sci.* 13 (2020) 4106–4113.
- [13] D. Hospital-Benito, J. Lemus, C. Moya, R. Santiago, V.R. Ferro, J. Palomar, Techno-economic feasibility of ionic liquids-based CO<sub>2</sub> chemical capture processes, *Chem. Eng. J.* 407 (2021), 127196.
- [14] C. Moya, R. Santiago, D. Hospital-Benito, J. Lemus, J. Palomar, Design of biogas upgrading processes based on ionic liquids, *Chem. Eng. J.* 428 (2022), 132103.
- [15] J. de Riva, V. Ferro, C. Moya, M.A. Stadtherr, J.F. Brennecke, J. Palomar, Aspen Plus supported analysis of the post-combustion CO<sub>2</sub> capture by chemical absorption using the P-2228 CNPyr and P-66614 CNPyr AHA ionic liquids, *Int. J. Greenhouse Gas Control* 78 (2018) 94–102.
- [16] B. Gurkan, B.F. Goodrich, E.M. Mindrup, L.E. Ficke, M. Massel, S. Seo, T.P. Senftle, H. Wu, M.F. Glaser, J.K. Shah, E.J. Maginn, J.F. Brennecke, W.F. Schneider, Molecular design of high capacity, low viscosity, chemically tunable ionic liquids for CO<sub>2</sub> capture, *J. Phys. Chem. Lett.* 1 (2010) 3494–3499.
- [17] G.M. Avelar Bonilla, O. Morales-Collazo, J.F. Brennecke, Effect of water on CO<sub>2</sub> capture by aprotic heterocyclic anion (AHA) ionic liquids, *ACS Sustain. Chem. Eng.* 7 (2019) 16858–16869.
- [18] Q.R. Sheridan, W.F. Schneider, E.J. Maginn, Role of Molecular modeling in the development of CO<sub>2</sub>-reactive ionic liquids, *Chem. Rev.* 118 (2018) 5242–5260.
- [19] S. Seo, M. Quiroz-Guzman, M.A. DeSilva, T.B. Lee, Y. Huang, B.F. Goodrich, W. F. Schneider, J.F. Brennecke, Chemically tunable ionic liquids with aprotic heterocyclic anion (AHA) for CO<sub>2</sub> capture, *J. Phys. Chem. B* 118 (2014) 5740–5751.
- [20] C. Moya, D. Hospital-Benito, R. Santiago, J. Lemus, J. Palomar, Prediction of CO<sub>2</sub> chemical absorption isotherms for ionic liquid design by DFT/COSMO-RS calculations, *Chem. Eng. J. Adv.* 4 (2020), 100038.
- [21] Y. Huang, G. Cui, H. Wang, Z. Li, J. Wang, Tuning ionic liquids with imide-based anions for highly efficient CO<sub>2</sub> capture through enhanced cooperations, *J. CO<sub>2</sub> Util.* 28 (2018) 299–305.
- [22] B. Hong, L.D. Simoni, J.E. Bennett, J.F. Brennecke, M.A. Stadtherr, Simultaneous process and material design for aprotic N-heterocyclic anion ionic liquids in postcombustion CO<sub>2</sub> Capture, *Ind. Eng. Chem. Res.* 55 (2016) 8432–8449.
- [23] D. Hospital-Benito, J. Lemus, C. Moya, R. Santiago, J. Palomar, Process analysis overview of ionic liquids on CO<sub>2</sub> chemical capture, *Chem. Eng. J.* 390 (2020), 124509.
- [24] K. Seo, C. Tsay, T.F. Edgar, M.A. Stadtherr, M. Baldea, Economic optimization of carbon capture processes using ionic liquids: toward flexibility in capture rate and feed composition, *ACS Sustain. Chem. Eng.* 9 (2021) 4823–4839.
- [25] S. Seo, M.A. DeSilva, H. Xia, J.F. Brennecke, Effect of cation on physical properties and CO<sub>2</sub> solubility for phosphonium-based ionic liquids with 2-cyanopyrrolide anions, *J. Phys. Chem. B* 119 (2015) 11807–11814.
- [26] H. Zhai, E.S. Rubin, Systems analysis of ionic liquids for post-combustion CO<sub>2</sub> capture at coal-fired power plants, *Energy Procedia* 63 (2014) 1321–1328.
- [27] V.R. Ferro, C. Moya, D. Moreno, R. Santiago, J. de Riva, G. Pedrosa, M. Larriba, I. Diaz, J. Palomar, Enterprise ionic liquids database (ILUAM) for use in aspen ONE programs suite with COSMO-based property methods, *Ind. Eng. Chem. Res.* 57 (2018) 980–989.
- [28] S.-T. Lin, S.I. Sandler, A priori phase equilibrium prediction from a segment contribution solvation model, *Ind. Eng. Chem. Res.* 41 (2002) 899–913.
- [29] G.D. Ulrich, P.T. Vasudevan, Chemical Engineering Process Design and Economics: A Practical Guide, Process Pub, 2004.
- [30] K. Xin, F. Gallucci, M.v.S. Annaland, Optimization of solvent properties for post-combustion CO<sub>2</sub> capture using process simulation, *Int. J. Greenhouse Gas Control* 99 (2020), 103080.
- [31] B.E. Gurkan, T.R. Gohndrone, M.J. McCready, J.F. Brennecke, Reaction kinetics of CO<sub>2</sub> absorption in to phosphonium based anion-functionalized ionic liquids, *Phys. Chem. Chem. Phys.* 15 (2013) 7796–7811.
- [32] D. Hospital-Benito, J. Lemus, R. Santiago, J. Palomar, Thermodynamic and kinetic evaluation of ionic liquids + tetraglyme mixtures on CO<sub>2</sub> capture, *J. CO<sub>2</sub> Util.* (2019).
- [33] B. Xue, Y. Yu, J. Chen, X. Luo, M. Wang, A comparative study of MEA and DEA for post-combustion CO<sub>2</sub> capture with different process configurations, *Int. J. Coal Sci. Technol.* 4 (2017) 15–24.
- [34] T.E. Akinola, E. Oko, M. Wang, Study of CO<sub>2</sub> removal in natural gas process using mixture of ionic liquid and MEA through process simulation, *Fuel* 236 (2019) 135–146.
- [35] J. Lemus, R. Santiago, D. Hospital-Benito, T. Welton, J.P. Hallett, J. Palomar, Process analysis of ionic liquid-based blends as H<sub>2</sub>S absorbents: search for thermodynamic/kinetic synergies, *ACS Sustain. Chem. Eng.* 9 (2021) 2080–2088.